

Structural Design Optimization of Movable-column Horizontal Machining Center Based on Integral Stiffness Analysis and Sensor Measurement

Kun-Chieh Wang and Chi-Hsin Yang*

College of Mechanical and Automotive Engineering, Zhaoqing University,
Zhaoqing City, Guangdong Province 526061, China

(Received September 12, 2022; accepted January 30, 2023)

Keywords: machine structural design, CNC machine tools, finite element analysis, horizontal machining center, vibration sensor, displacement sensor

Owing to the requirement of ever-increasing machining accuracy in tool machinery, the research on how to optimally design a reliable high-rigidity computer-numerical-controlled (CNC) machine tool is increasing in importance. Conventionally, machine designers carried out design optimization by attempting to maximize only the static stiffness. Nowadays, for high-precision machining, a good machine tool should have high rigidity not only under static stimuli but also under dynamic stimuli. The dynamic rigidity of the machine structure is thus receiving increasing attention. In this study, we propose an integral-stiffness-based optimization methodology for designing the optimal structure of a CNC horizontal machining center (HMC). The proposed novel optimization methodology is mainly based on Taguchi's experimental method, the finite element method (FEM), and gray relational analysis (GRA). In addition, some specifically designed experiments on machine stiffness are performed using displacement sensors to verify the calculation results. The optimization parameters consist of the static stiffness, the first natural frequency, and the dynamic stiffness. Through the use of our proposed methodology, the optimal structural dimensions of the target HMC that give high integral rigidity can be determined. Moreover, the proposed optimization methodology provides a good guide for machine designers to design the high-rigidity structure of a CNC machine tool efficiently and accurately.

1. Introduction and Literature Review

With the requirement of higher dimensional accuracy for complex metal workpieces in the car, cell phone, and mold-making industries, the research on how to optimally design reliable high-rigidity computer-numerical-controlled (CNC) machine tools is attracting increasing attention. Specifically, CNC horizontal machining centers (HMCs) have been developed for machining as many metal workpieces as accurately as possible in one clamping. However, high-

*Corresponding author: e-mail: m18316252648@163.com
<https://doi.org/10.18494/SAM4117>

precision machining is not easy to attain for an HMC since its structure is asymmetric and complicated, and the design of the optimal structure for such HMCs remains a challenge.

When a machine tool is in operation, a cutting force is induced between the tool and the workpiece. This cutting force comprises two types of force. One is the static force, which may affect the geometric accuracy of the workpiece. The other is the dynamic force, which may affect the surface roughness of the workpiece. Deformation may occur when the machine structure is subject to cutting forces. For a machine tool, the static stiffness is defined as the applied static force divided by its resultant deformation, and the dynamic stiffness is defined as the applied dynamic force divided by its resultant deformation. Conventionally, machine designers have only been concerned with static stiffness. However, with the increasing demands regarding machining accuracy, the deformation induced by dynamic stimuli or resonance can no longer be ignored and should be considered seriously. Therefore, the goal of the structure optimization of a machine tool should be to obtain high static stiffness as well as high dynamic stiffness, but the variation of the machine weight should be controlled within a suitable range. These requirements result in the need to design machine structures with high resistance to the applied static and dynamic forces. There have been many studies on the structure optimization of components in a machine tool, such as the spindle, bed, and column.^(1–3) Heng *et al.*⁽⁴⁾ employed a topology optimization method to improve the rigidity of the rib plate in a machine's column. Liusheng *et al.*⁽⁵⁾ investigated the optimization problem of a lathe bed using dynamic characteristic analysis. In short, previous studies adopted optimization schemes based on a structure analogy, the finite element method (FEM), and experience-based design, where only static stiffness was considered.^(6–10) Regarding the high structural strength required for modern precision tool machinery, the existing machine-structure design methodologies are far from sufficient. Furthermore, many investigations on structure optimization problems for modules or whole machines have been reported. For example, Lei *et al.*⁽¹¹⁾ used the modal strain energy sensitivity to optimally design the bed structure of a CNC machine tool. Jie⁽¹²⁾ studied a lightweight structural optimization design system for a gantry machine tool. Guodong *et al.*⁽¹³⁾ investigated the design schemes of reconfigurable machine tools based on multiple-attribute decision-making. Wang *et al.*⁽¹⁴⁾ designed and developed a five-axis machine tool with high stiffness. Liu *et al.*⁽¹⁵⁾ studied the optimization problem of an electrical discharge machining (EDM) machine tool based on computer-assisted engineering (CAE) simulations. Lin *et al.*⁽¹⁶⁾ explored a suitable method of optimally designing an HMC. Ta *et al.*⁽¹⁷⁾ studied the optimization design problem of CNC machine tools by a multidisciplinary approach. Wu *et al.*⁽¹⁸⁾ proposed a tolerance modeling method to increase the static geometric accuracy of a machine tool. Recently, with the development of highly rigid machine structures, increasing importance has been attached to the dynamic responses of machines.^(19,20) In summary, the optimal consideration of both the static and dynamic stiffnesses of the machine structure is a prerequisite for designing a good machine tool.

For machine tools, the static and dynamic stiffnesses are the most crucial parameters affecting their machining accuracy. The static stiffness represents the resistance to deformation when the machine is subject to a static force. The modal shapes of a machine are the resultant

deformations under free oscillations at different natural frequencies, which may provide an insight into the machine resonance. The dynamic stiffness represents the dynamic response of a machine under periodic stimuli of external forces. The above three parameters of static stiffness, natural frequency, and dynamic stiffness mutually affect each other. Sometime a high-static-stiffness machine exhibits large dynamic deformations or, even more seriously, damage due to resonance or certain applied dynamic stimuli. Thus, an integrative investigation on the effect of these three parameters is of marked importance in optimally designing machine tools.

With the above background, in this study, we propose a novel integral-stiffness-based methodology that mainly considers the effects of the three parameters to solve the structure optimization problem of a target HMC. We adopt the well-known Taguchi's experimental method,⁽²¹⁾ also known as the factorial design of experiments, which may effectively reduce the required number of experiments while still capturing the effects of controlled variables on target variables. To verify our simulation results, we perform some experiments to measure a machine's static stiffness using some displacement sensors. The proposed integral-stiffness-based optimization scheme is mainly based on FEM, Taguchi's experimental method, and gray relational analysis (GRA). Details are addressed in the following section.

2. Optimization Procedure

Our proposed integral-stiffness-based optimization methodology mainly consists of seven steps, as illustrated in Fig. 1. Step 1: We select a CNC HMC as the target machine since its structure is highly asymmetric and complicated. Its major structural components are a long T-type base with a working table on it and a movable, vertical, and rectangular hollow column with a horizontal ram inside it. There is also a milling spindle installed inside the ram. Although this type of HMC has the advantages of high efficiency and precision in machining, being capable of four-face machining in one clamping, it is prone to large deformations when subject to cutting forces owing to its complicated and asymmetric structure. This type of machine thus provides a good opportunity to test our proposed structure optimization methodology. Step 2: We develop a prototype HMC based on past design experiences. Step 3: We establish a set of Taguchi's orthogonal arrays (OAs) to study the effects of structure-shape parameters on the machine stiffness. Then, the static and dynamic responses of the HMC are investigated via FEM in Steps 4 and 5, respectively. Step 6: We propose the concept of integral stiffness and accordingly analyze previous results via GRA to obtain an optimal structure for the HMC. Step 7: We verify the optimal structure via experimental measurements of the machine's static deformation using displacement sensors.

3. Theoretical Background

Our proposed integral-stiffness-based optimization methodology comprises four theories: solid mechanics, Taguchi's experimental method, FEM, and GRA. Details are given as follows.

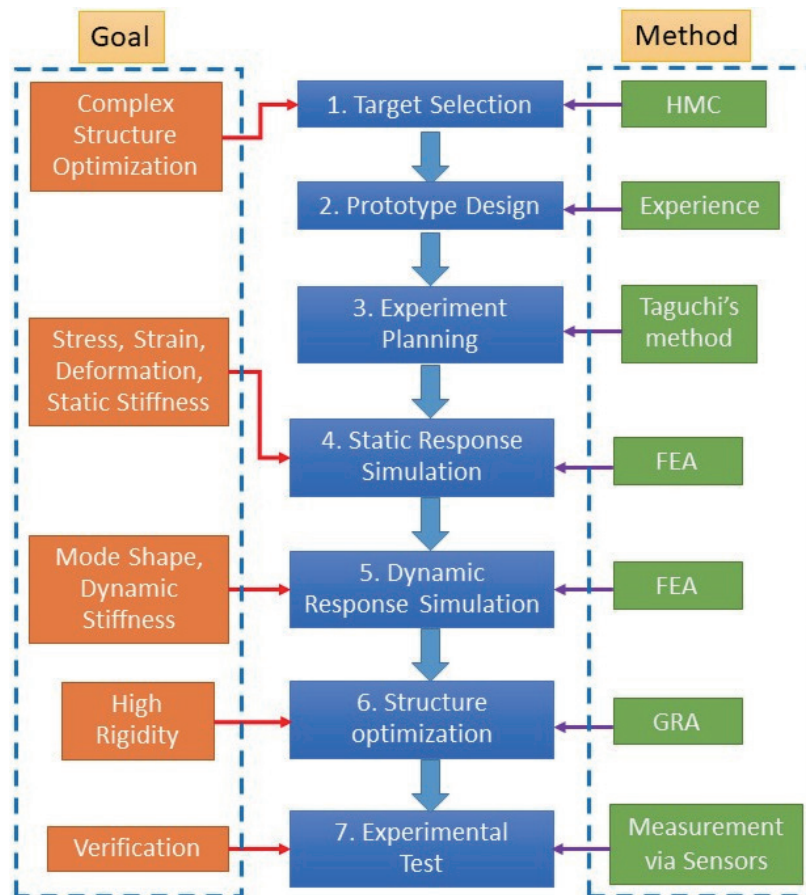


Fig. 1. (Color online) Flow chart of proposed integral-stiffness-based optimization methodology.

3.1 Solid mechanics and finite element method

3.1.1 Finite element method

FEM is a popular method of analyzing the structural parameters of a machine tool, such as stress, strain, and displacement.^(22–26) Many calculation software packages have been developed for FEM applications, such as CREO, ANSYS, and NASTRAN^(27,28) Among them, ANSYS shows good calculation performance in analyzing various physical problems.^(29–33)

In this study, we adopt ANSYS for FEM calculations. The procedure in ANSYS mainly consists of three steps: (1) a pre-processing phase: establishing the solution domain, selecting shape functions, calculating the global stiffness matrix, and applying restrictions; (2) a solution phase: solving governing equations to acquire the nodal displacement, strain, and stress; (3) a post-processing phase: calculating natural frequencies and stiffness and plotting deformation figures.

3.1.2 Principles of mechanics

Static Response: When a load is applied to a certain body, the force balance equation can be expressed in matrix form as

$$[K]\{Y\} = \{F\}, \quad (1)$$

or

$$[K]\{Y\} = \{F_e\} + \{F_r\}, \quad (2)$$

where $[K] = \sum_{i=1}^n [K_s]$ is the stiffness matrix of the system; $\{Y\}$ is the displacement vector; n is the number of elements; $[K_s]$ is the stiffness matrix of the elements; $\{F_r\}$ and $\{F_e\}$ are the reaction load vector and the total external force vector, respectively.

Modal analysis: In modal analysis, it is assumed that there is no damping effect, the structure material is linear in its elasticity, and none of the physical properties change with time. Since there is no actual force applied to the structure, the structure is under free oscillation. The governing equation is

$$[M]\{\ddot{Y}\} + [K]\{Y\} = \{0\}, \quad (3)$$

where $[M]$ is the mass matrix of the system. Since the motion of the structure is harmonic, we may assume that the displacement has the form

$$\{Y\} = \{Y\}_i e^{j\omega_i t}, \quad (4)$$

where $[Y]_i$ is the amplitude for the i th frequency ω_i . Substituting Eq. (4) into Eq. (3), we have

$$\left[[K] - \omega_i^2 [M] \right] \{Y\}_i = \{0\}. \quad (5)$$

This is an eigenvalue problem. Non-trivial solutions exist when

$$\det\left(\left[[K] - \omega_i^2 [M] \right]\right) = 0. \quad (6)$$

From Eq. (6), we may obtain the natural frequencies $\{\omega_i\}$ and their corresponding modal shapes $[Y]_i$.

Dynamic response: Supposing that a time-variant force $\{F(t)\}$ is applied to a structure, the governing equation of the force balance can be written as

$$[M]\{\ddot{Y}\} + [C]\{\dot{Y}\} + [K]\{Y\} = \{F(t)\}, \quad (7)$$

where $[C]$ is the damping matrix. We assume

$$\{F(t)\} = \{F_{max} e^{i\psi}\} e^{i\omega t} \quad (8)$$

and

$$\{Y\} = \{Y_{max} e^{i\phi}\} e^{i\omega t}, \quad (9)$$

where F_{max} is the maximum external force, ψ is the phase angle of the force, Y_{max} is the maximum displacement, and ϕ is the phase angle of the displacement. Substituting Eqs. (8) and (9) into Eq. (7), we obtain the final equation of the structural dynamic response as

$$\left(-\omega^2 [M] + i\omega [C] + [K]\right) \{Y_{max} e^{i\phi}\} = \{F_{max} e^{i\psi}\}. \quad (10)$$

The displacement vector of the dynamic response $\{Y_{max} e^{i\phi}\}$ is obtained by solving Eq. (10).

3.2 Taguchi's experimental method

In experimental studies, there are usually many influential factors. To reduce the number of experiments, we adopt Taguchi's experimental method,⁽²¹⁾ which is a factorial design of experiments. An experimental method of obtaining the maximum amount of information by choosing a limited number of experiments is defined as the partial factorial experiment (PFE). Taguchi's experimental method adopts a set of OAs in PFE. Usually, there are two, three, or at most four levels in an OA. Taguchi's experimental method comprises four steps: 1. determination of influential parameters; 2. design of experiments; 3. parameter analysis; 4. confirmatory test.

3.3 GRA

GRA is a frequently used correlation analysis method for discrete data sequences and a powerful tool in dealing with insufficient data. The procedure of GRA is illustrated as follows.⁽³⁴⁾

Step 1: Establish the initial data sequence

$$\begin{cases} x_1^{(0)} = \{x_1^{(0)}(1), x_2^{(0)}(2), \dots, x_1^{(0)}(m)\} \\ x_2^{(0)} = \{x_2^{(0)}(1), x_2^{(0)}(2), \dots, x_2^{(0)}(m)\} \\ \dots \\ x_n^{(0)} = \{x_n^{(0)}(1), x_n^{(0)}(2), \dots, x_n^{(0)}(m)\} \end{cases}. \quad (11)$$

Step 2: Normalize this initial data sequence as

$$x_i^*(k) = \frac{x_i^{(0)}(k)}{\eta}, \quad i = 1, 2, \dots, n; \quad k = 1, 2, \dots, m, \quad (12)$$

where η is the initial value, $\eta = x_i^{(0)}(1)$, and $X_i^* = \{x_i^*(k)\}$.

Step 3: Choose a data sequence of X_0^* from X_i^* as follows:

$$X_0^*(k) = \{x_0^*(1), x_0^*(2), \dots, x_0^*(m)\}. \quad (13)$$

Step 4: Obtain the norm sequence $\Gamma_i = \{\Delta_{0i}(1), \Delta_{0i}(2), \dots, \Delta_{0i}(m)\}$ whose element is the absolute value of the difference between the data and the initial sequence, i.e.,

$$\Delta_{0i}(k) = \|x_0^*(k) - x_i^*(k)\|. \quad (14)$$

Step 5: Calculate the extreme values of the above norm sequences:

$$\alpha = \max_{i=1}^n \max_{k=1}^m \Delta_{0i}(k), \quad \beta = \min_{i=1}^n \min_{k=1}^m \Delta_{0i}(k). \quad (15)$$

Step 6: Calculate the gray relational coefficient

$$\gamma_{0i}(k) = \frac{\beta + \lambda \cdot \alpha}{\Delta_{0i}(k) + \lambda \cdot \alpha}, \quad \lambda \in [0, 1], \quad (16)$$

where λ is the distinguishing coefficient, which represents the contrast between the measured and reference data. Usually, λ is chosen as 0.5.

4. Results and Discussion

4.1 Static and dynamic responses of prototype

The prototype of our target HMC is initially designed by professional designers with over a decade of experience in developing CNC machine tools. This prototype (Case 1) is shown in Fig. 2.

4.1.1 Restricted conditions and grid-independent tests

Three forces with a magnitude of 100 Kg_f are applied to the spindle tip in the X, Y, and Z directions as shown in Fig. 3. The structure material is chosen as graphite cast iron. In mesh

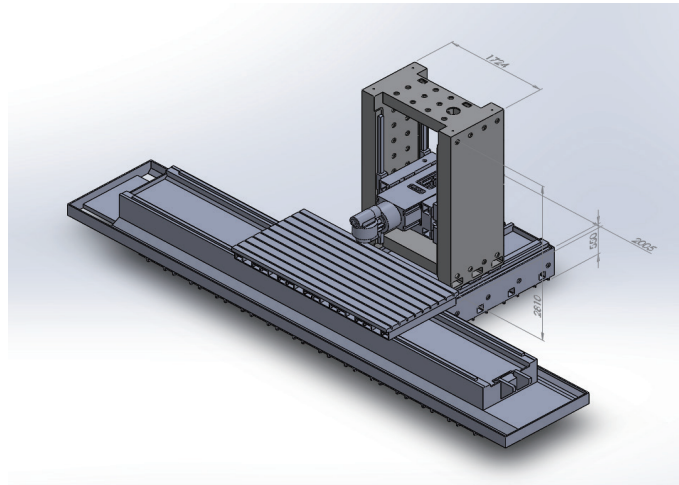


Fig. 2. (Color online) Configuration of HMC prototype.

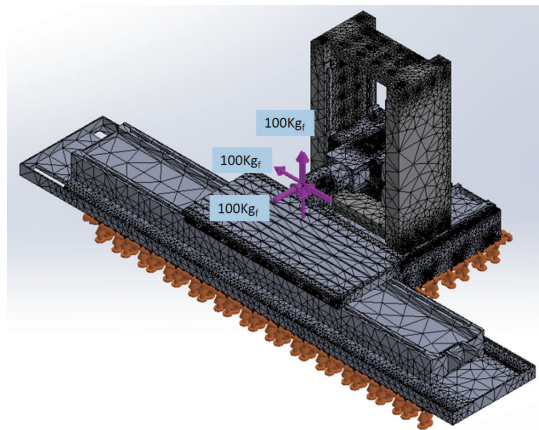
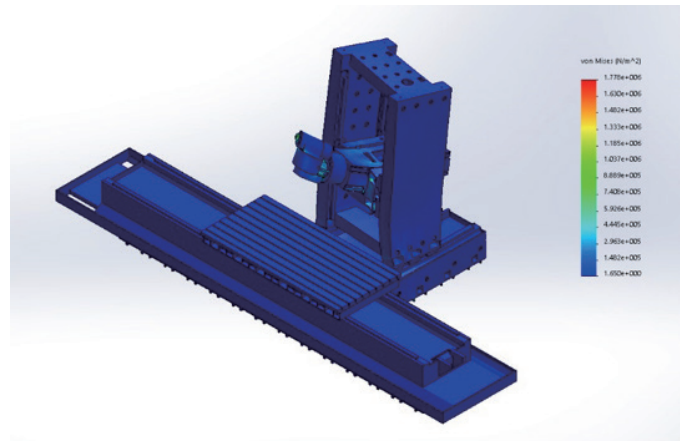


Fig. 3. (Color online) Meshing result and applied forces in Case 1.

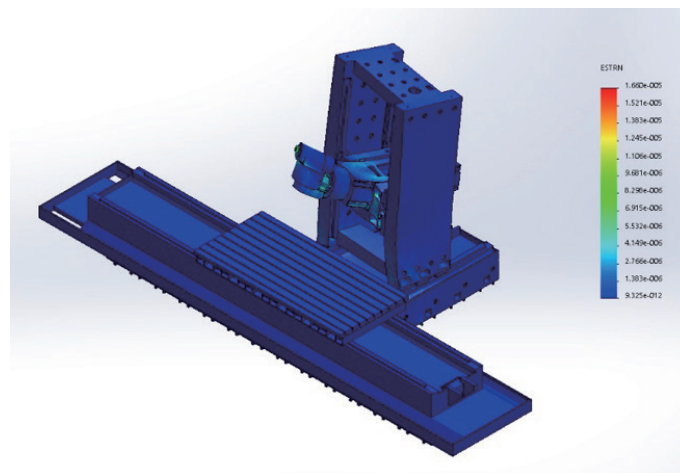
independence tests, a total of four different meshes with sequentially minimal mesh element sizes of 10, 7.5, 5, and 2.5 mm are chosen. We find that the relative deviations of the first natural frequency between the first three mesh elements and the final mesh elements are 0.81, 0.49, and 0.04 %, respectively. Therefore, we can choose the minimal mesh element size of 5 mm as the calculation basis in the following FEM calculations to reduce computation time while maintaining accuracy. A meshing result of the HMC prototype with 1058037 nodes and 555020 elements is shown in Fig. 3.

4.1.2 Static stiffness

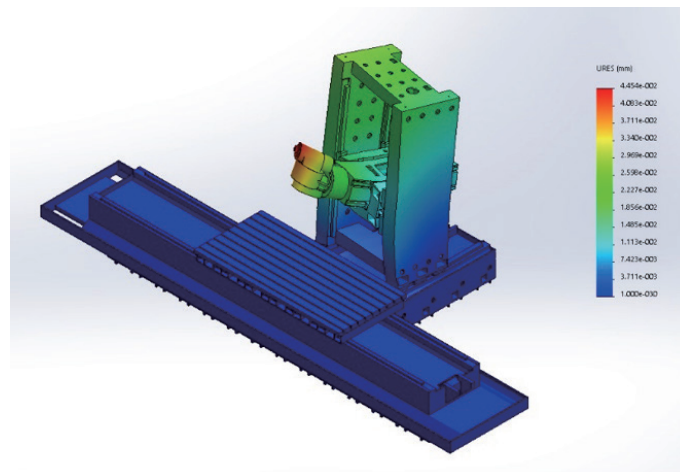
Through FEM calculations, we obtain the static stress, strain, and displacement distributions of the target HMC in Case 1. Sketch maps of the distributions for these parameters are shown in Fig. 4. A maximal displacement of 44.53 μm appears at the tip of the horizontal spindle [Fig. 4(c)]. The static stiffness of the whole machine is defined as $K_s = F_s / \delta_1$, where F_s is the



(a)



(b)



(c)

Fig. 4. (Color online) Static stress, strain, and displacement distributions in Case 1. (a) Stress distribution in Case 1, (b) strain distribution in Case 1, and (c) displacement distribution in Case 1.

applied static resultant force and δ_1 is the corresponding maximal displacement. Accordingly, we may calculate the total static stiffness of the target HMC as $K_s = 3.89 \text{ Kg}_f / \mu\text{m}$. A maximal von Mises stress of 44.5 MPa [Fig. 4(b)] and a maximal strain of 1.66×10^{-5} [Fig. 4(a)] are also found to appear at the same tip position of the horizontal spindle. The obtained displacements of module parts for our target HMC can be expressed in descending order as

$$\delta_{spindle} > \delta_{ram} > \delta_{column} > \delta_{bed} . \quad (17)$$

The spindle head obviously has the greatest deformation among all module components. Since the static stiffness represents the robustness of a machine under the applied static force, here we choose K_s as one of the structural optimization parameters, where a larger value is better.

4.1.3 Mode shape

The mode shape analysis of the natural oscillation in a machine may provide a clear insight into the bias of the dynamic interaction at the interface between module components. The rigidity of a whole machine may be modified through the useful dimension data obtained by investigating the deformation types of different mode shapes and the fragile parts of the machine structure.

We now calculate the natural frequencies of the target HMC via Eqs. (3)–(6). The first 50 natural frequencies (M1–M50) obtained are shown in Fig. 5 and the first 10 mode shapes obtained are shown in Fig. 6. For example, the first two mode shapes (M1 and M2) show that the vertical column deforms forth and back at $f = 24.0 \text{ Hz}$ and $f = 25.8 \text{ Hz}$. The third mode shape (M3, $f = 39.3 \text{ Hz}$) corresponds to an upward deformation of the bed at the left end. The fourth mode shape (M4, $f = 44.5 \text{ Hz}$) represents a type of clockwise-twist deformation of the vertical column. The fifth mode shape (M5, $f = 59.3 \text{ Hz}$) corresponds to an upward deformation of the

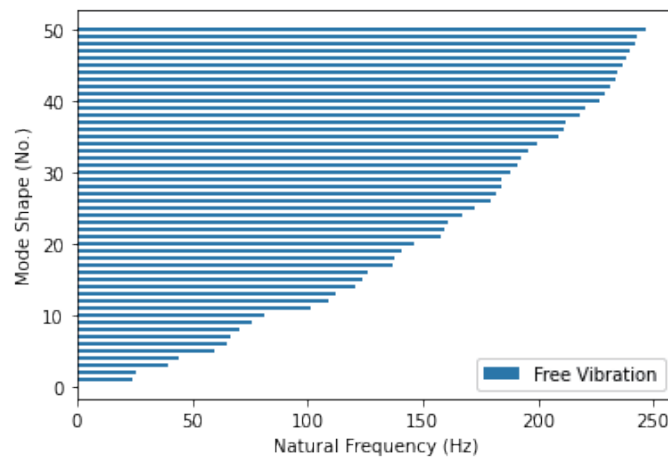


Fig. 5. (Color online) Natural frequencies of free vibration in Case 1.

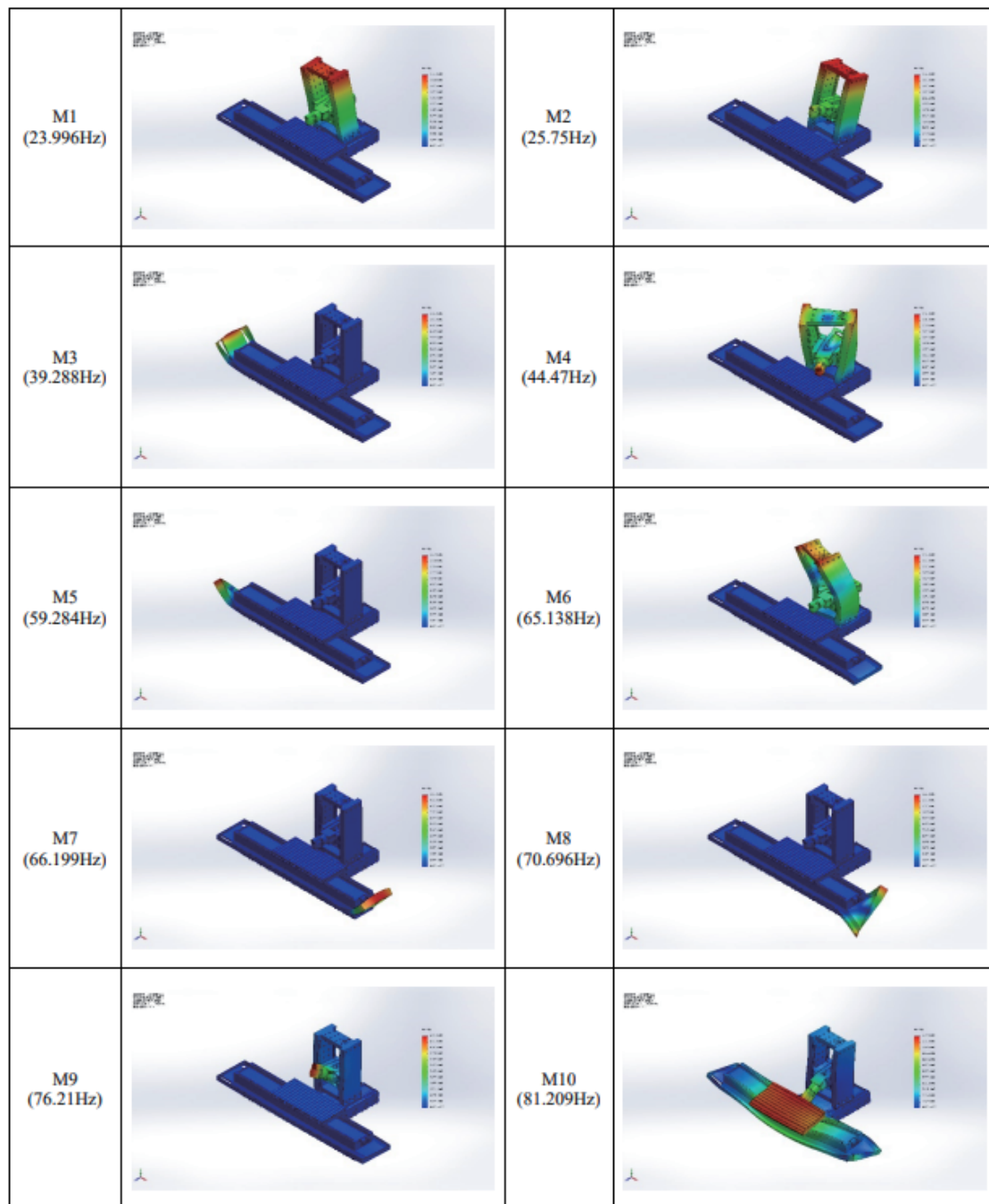


Fig. 6. (Color online) First ten mode shapes in Case 1.

bed at the right end. The sixth mode shape (M6, $f = 65.1$ Hz) represents a type of counterclockwise-twist deformation of the vertical column. From the first six mode shapes that frequently appear during machine operations, it is found that the dimension parameters of the vertical column and the base are crucial factors in designing a high-rigidity machine. Accordingly, in Taguchi's experimental method, we may set the dimension variations of the

modular components as column length CL (three levels: 2810, 3091, and 3372 mm), column width CW (three levels: 1724, 1896.4, and 2068.8 mm), base height BH (three levels: 550, 605, and 660 mm), and base width BW (three levels: 2005, 2205.5, and 2406 mm). On the basis of resonance considerations, we choose the first natural frequency of the whole machine structure, denoted by f_s , as one of the structural optimization parameters, where a smaller value is better.

4.1.4 Dynamic response

Using Eqs. (7)–(10), we now calculate the dynamic response of the target HMC under the stimuli of periodically applied forces. Three dynamic forces of 100 Kg_f are applied to the spindle tip in the X , Y , and Z directions with harmonic frequencies in the range between 0 and 500 Hz. The obtained variation of the maximal deformation with the frequency is shown in Fig. 7. Two deformation peaks of 486 and 378 μm are found at 35.9 and 148.4 Hz, respectively. External stimuli with frequencies similar to these two frequencies will induce large deformations or even failure during machining. The dynamic stiffness of the target HMC can then be calculated via the formula $K'_d = F_d / \delta_d$, where F_d is the applied harmonic force and δ_d is its corresponding maximal deformation at a certain stimulus frequency. The obtained variation of the dynamic stiffness with the stimulus frequency is shown in Fig. 8. The global maximal dynamic stiffness is found to be $K'_d = 0.356 \text{ kgf}/\mu\text{m}$ at 35.9 Hz, which can be defined as the “total dynamic stiffness”, and denoted by K_d . Consequently, we choose K_d as one of the structural optimization parameters, where a larger value is better.

4.1.5 Experimental verification

To verify the simulation results, we now perform a deformation measurement. The experimental setup mainly includes a load cell and some displacement sensors, as shown in

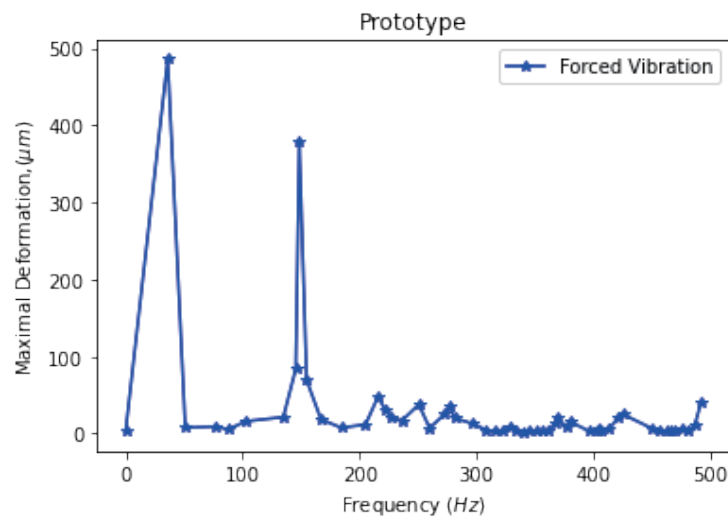


Fig. 7. (Color online) Maximal deformation distribution in Case 1.

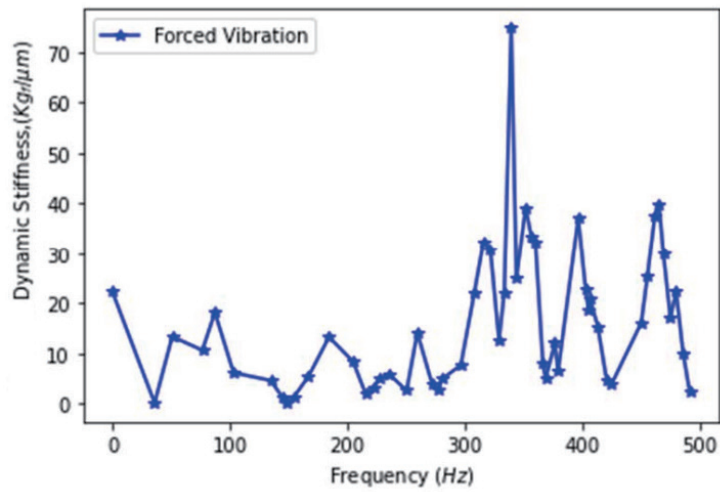


Fig. 8. (Color online) Dynamic stiffness distribution in Case 1.

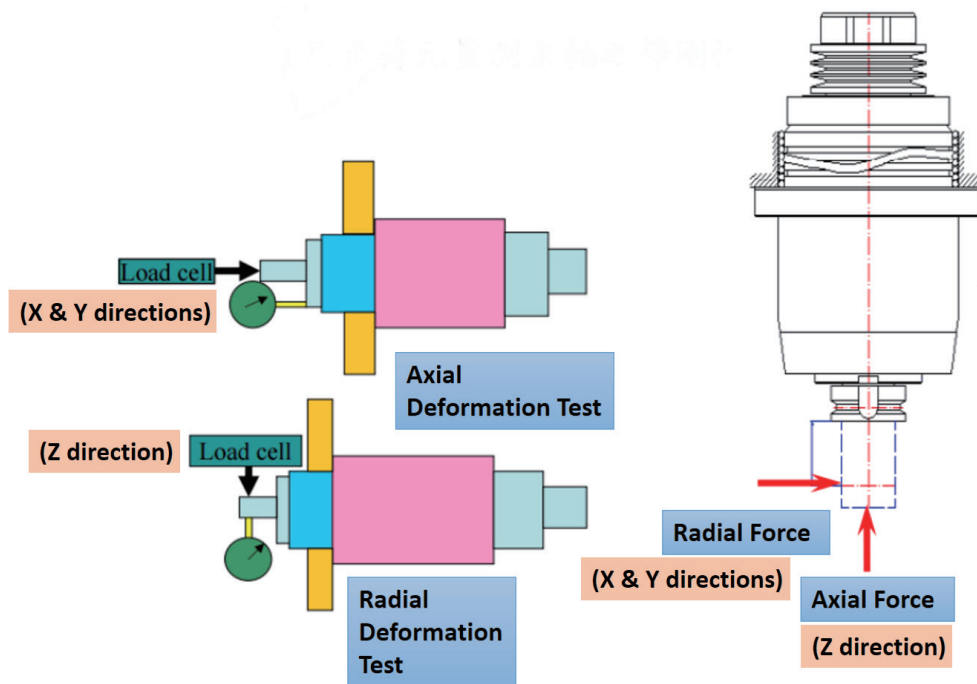


Fig. 9. (Color online) Setup of deformation measurement system.

Fig. 9. Six sensors of the strain gauge are attached to the front end of the horizontal spindle head to measure the deformation induced by the applied static force. We then apply forces of 100 kgf in the *X*, *Y*, and *Z* directions at the front end of the spindle through the load cell. The measured total composite deformation is 48.06 μm, which differs from the simulation result by 3.53 μm. Therefore, we infer that the following simulation results are satisfactory.

4.2 Taguchi's experimental method

On the basis of the previous discussion, we now choose three parameters as the decision factors for optimization: the total static stiffness at the spindle nose (K_s), the first natural frequency (f_s), and the total dynamic stiffness (K_d). Four shape parameters, CL , CW , BH , and BW , are chosen as the controlled factors, and each controlled factor has three levels, as given in Sect. 4.1.3. Accordingly, we construct a Taguchi's orthogonal array of $L_9(3^4)$, and only nine cases must be examined experimentally, as shown in Table 1.

4.3 Structure optimization

4.3.1 Optimization based on static rigidity

We first calculate the displacement, stress, and strain distributions via FEM in all nine cases. The obtained maximal deformations, occurring at the spindle tip, in all cases are shown in Table 2. Case 6 has the smallest δ_s of 0.0406 μm , which means that this case has the largest total static stiffness of $K_s = 4.98$. To examine the effects of the shape parameters in greater depth, we define the signal-to-noise ratio as

Table 1
Taguchi's orthogonal array of $L_9(3^4)$. (unit: mm)

Experiment	CL	CW	BH	BW
Case 1	2810 (level 1)	1724 (level 1)	550 (level 1)	2005 (level 1)
Case 2	2810 (level 1)	1896.4 (level 2)	605 (level 2)	2205.5 (level 2)
Case 3	2810 (level 1)	2068.8 (level 3)	660 (level 3)	2406 (level 3)
Case 4	3091 (level 2)	1724 (level 1)	605 (level 2)	2406 (level 3)
Case 5	3091 (level 2)	1896.4 (level 2)	660 (level 3)	2005 (level 1)
Case 6	3091 (level 2)	2068.8 (level 3)	550 (level 1)	2205.5 (level 2)
Case 7	3372 (level 3)	1724 (level 1)	660 (level 3)	2205.5 (level 2)
Case 8	3372 (level 3)	1896.4 (level 2)	550 (level 1)	2406 (level 3)
Case 9	3372 (level 3)	2068.8 (level 3)	605 (level 2)	2005 (level 1)

Table 2
Results of Taguchi's experimental method.

Experiment	CL	CW	BH	BW	δ_s (μm)	Ω
Case 1	2810	1724	550	2005	0.0445367	-27.026
Case 2	2810	1896.4	605	2205.5	0.0437095	-27.188
Case 3	2810	2068.8	660	2406	0.0407841	-27.790
Case 4	3091	1724	605	2406	0.0436339	-27.204
Case 5	3091	1896.4	660	2005	0.0408882	-27.768
Case 6	3091	2068.8	550	2205.5	0.0347558	-29.179
Case 7	3372	1724	660	2205.5	0.0432528	-27.280
Case 8	3372	1896.4	550	2406	0.0419602	-27.543
Case 9	3372	2068.8	605	2005	0.0406196	-27.825

$$\Omega = 10 \log_{10} \delta_s^2, \quad (18)$$

where a smaller value is better. From the data of δ_s listed in Table 2, we obtain the signal-to-noise ratio in all cases via Eq. (17) and then calculate the effects of the four controlled parameters on the signal-to-noise ratio (shown in Table 3). It can be seen from Table 3 that, among all shape parameters, CW has the largest effect on the structure deformation. This finding provides the design guide that a change in CW (where a larger value is better) is an effective way to enhance the rigidity of the machine. Furthermore, the effects of the four shape parameters decrease in the order $CW > CL > BH > BW$. Moreover, the HMC with the following shape parameters and levels will exhibit the greatest static rigidity among all cases.

$$CL = 3091 \text{ mm (level 2)}, CW = 2068.8 \text{ mm (level 3)}, BH = 550 \text{ mm (level 1)}, BW = 2205.5 \text{ mm (level 2)} \quad (19)$$

As expected, this corresponds to Case 6, which has the smallest δ_s among the cases.

4.3.2 Optimization based on integral stiffness

In addition to the static rigidity, we must also consider the dynamic rigidity of the machine. Through FEA, we obtain K_s , f_s , and K_d in the above nine cases, as listed in Table 4. Case 6 has the largest total static stiffness of $K_s = 4.98 \text{ kgf}/\mu\text{m}$ (the larger the better) and the largest first natural frequency of $f_s = 42.78 \text{ Hz}$ (the larger the better), but Case 8 has the greatest total dynamic stiffness of $K_d = 0.531 \text{ kgf}/\mu\text{m}$. There is clearly a structure–performance conflict

Table 3
Effects of controlled parameters on signal-to-noise ratio.

Level	CL	CW	BH	BW
Level 1	-27.335	-27.17	-27.916	-27.540
Level 2	-28.050	-27.412	-27.406	-27.882
Level 3	-27.549	-28.598	-27.613	27.512
Influence	0.715	1.428	0.51	0.37

Table 4
FEM simulation results of K_s , f_s , and K_d in cases 1–9.

Cases	K_s (kgf/ μm)	f_s (Hz)	K_d (kgf/ μm)
1	3.89	23.00	0.356
2	3.96	28.12	0.411
3	4.25	32.63	0.455
4	3.97	34.51	0.477
5	4.24	39.52	0.489
6	4.98	42.78	0.516
7	4.00	29.11	0.522
8	4.13	35.42	0.531
9	4.26	31.89	0.399

between the static and dynamic responses of our target HMC. Although the HMC in Case 6 has the highest total static stiffness, it has only the third highest total dynamic stiffness.

To clarify the overall structural performance of the HMC in all cases, we now introduce the concept of integral stiffness. We simultaneously consider three stiffness parameters: K_s (static strength of machine), f_s (first part of dynamic strength of machine), and K_d (second part of dynamic strength of machine). Then, we apply GRA to clarify in greater depth the structural strength of the HMC based on the integral stiffness.

First, we normalize the data listed in Table 4 using Eq. (12). Second, we calculate the difference in the normalized data using Eq. (14). Finally, we calculate the gray relational coefficients in all nine cases using Eq. (16). The obtained result is shown in Fig. 10. Case 6 has the highest gray relational coefficient of 0.983. From the viewpoint of integral stiffness, Case 6 has an optimal structure that performs well in the three aspects of static response, resonance, and dynamic response. Case 5 (gray relational coefficient: 0.958) and Case 9 (gray relational coefficient: 0.97) also have high integral stiffness. Note that an optimal machine structure may have high static rigidity but low dynamic rigidity or vice versa. Consequently, to design a suitable machine structure, it is important to consider the integral stiffness (including the static stiffness, first natural frequency, and dynamic stiffness).

4.4 Dynamic response of optimal structure of HMC

Since Case 6 has an optimal structure, we now study its dynamic response in greater depth. The FEM-obtained variations of the maximal deformation and the corresponding dynamic stiffness distribution with the frequency are shown in Figs. 11 and 12, respectively. It is seen from Fig. 12 that two large peak deformations of 148 and 105 μm appear at 40.0 and 149.6 Hz, respectively. Note that when operating around these two frequencies, our target HMC will exhibit abnormal oscillations, inducing large machining errors or, worse, damage to machine

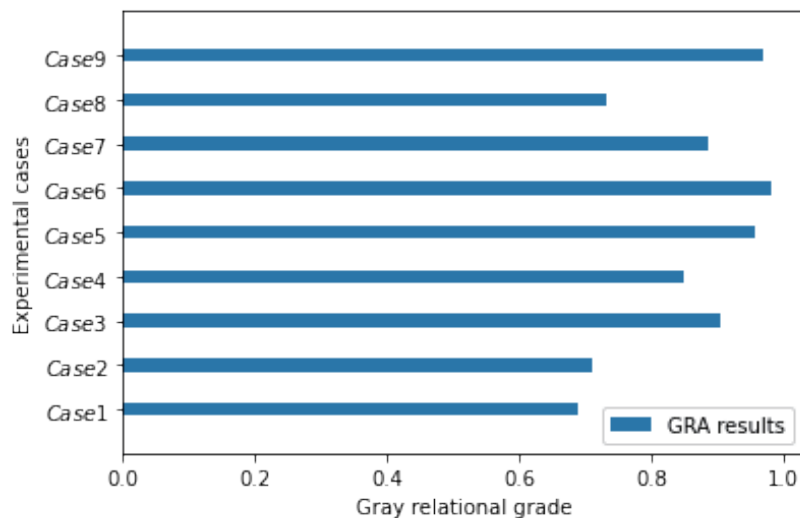


Fig. 10. (Color online) Gray relational grades of all experimental cases.

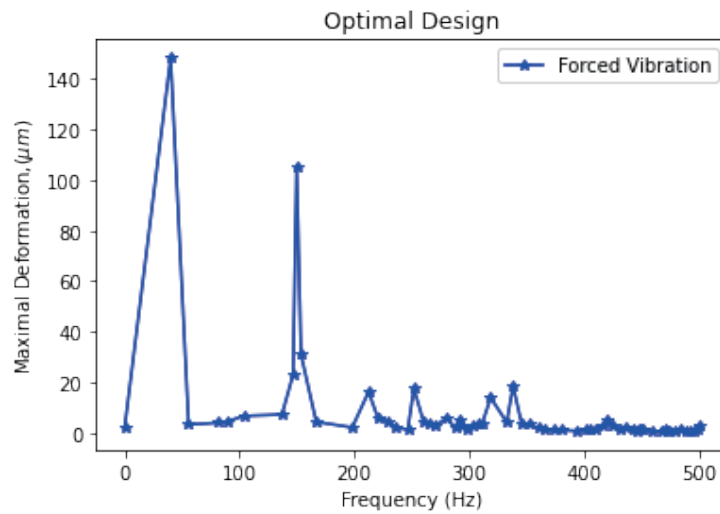


Fig. 11. (Color online) Maximal deformation distribution for optimal structure (Case 6).

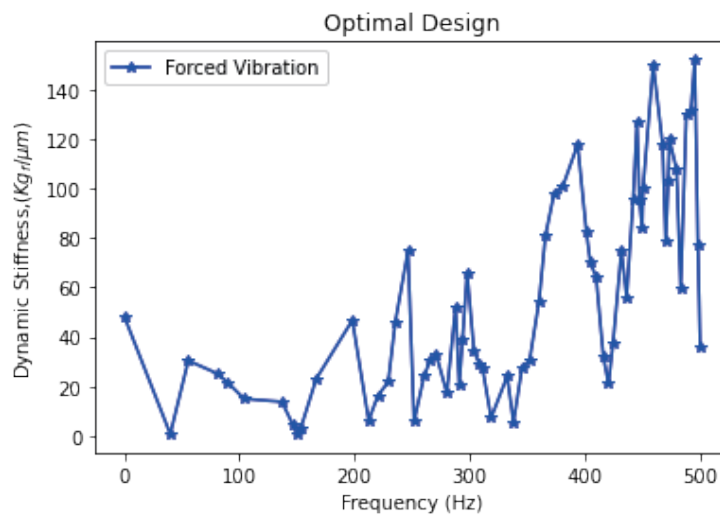


Fig. 12. (Color online) Dynamic stiffness distribution for optimal structure (Case 6).

parts. Compared with the peak deformations in Case 1 (486 and 378 μm), the two peak values in Case 6 (148 and 105 μm) are much smaller. The largest total dynamic stiffness is found in Case 8 ($K_d = 0.531$) among the nine cases.

4.5 Verification and comparison

We compare the results of this study with those of a previous study on the static and dynamic rigidities of a CNC machine tool. Wagner⁽²⁸⁾ investigated a design optimization method based on the static stiffness of a grinding machine. They found that for the considered grinding machine, the maximum static deformation was 13.1 μm , slightly less than the maximum static



Fig. 13. (Color online) Final HMC optimized via the proposed design methodology.

deformation of 143 μm in Case 6 in this study. In contrast, the optimal target structure in the previous study had a maximum dynamic deformation of 486 μm at 35.9 Hz, compared with only 148 μm at 40 Hz in this study. A deviation between the static and dynamic rigidities commonly exists for machine tools. The goal of this study to find an appropriate design methodology to optimally design a highly rigid machine by simultaneously considering the static and dynamic rigidities. Through the use of our proposed integral-stiffness-based methodology, a new highly rigid CNC HMC is expected to be realized, as shown in Fig. 13.

5. Conclusion

In this research, a novel integral-stiffness-based methodology is proposed to optimally design a CNC HMC with high rigidity. Starting from a prototype structure designed on the basis of experience, we examine the static and dynamic stiffnesses of the target HMC and find the possible variation of the shape parameters of the structure for optimization. Then, we construct Taguchi's orthogonal array of L_9 (3^4) and perform nine FEM simulation experiments. Through GRA, it is found that Case 6 has the optimal structure. Although Case 8 has the greatest total dynamic stiffness, it does not have the greatest overall structure performance. To verify the calculation results, we perform some measurement experiments on machine stiffness using strain gauge sensors. We also compare the static stiffness with those of other types of machine. Although the static stiffness is a conventionally considered factor that significantly affects the deformation of a machine during machining, a full consideration of the whole static stiffness, the first natural frequency, and the whole dynamic stiffness of the machine is a more appropriate way to design a highly rigid CNC machine tool.

Acknowledgments

The authors acknowledge the support from College of Mechanical and Automotive Engineering, Zhaoqing University.

References

- 1 C. Liu, T. Feng, L. Wang, and C. Zhaoyong: *J. Mech. Eng.* **52** (2016) 161. <https://doi.org/10.3901/JME.2016.03.161>
- 2 Z. Ting: *Forging Stamping Technol.* **35** (2010) 74.
- 3 Y. Altintas and Y. Cao: *CIRP Annals* **54** (2005) 379. [https://doi.org/10.1016/S0007-8506\(07\)60127-9](https://doi.org/10.1016/S0007-8506(07)60127-9)
- 4 J. Heng, G. Yisheng, and Q. Zhicheng: *J. Mech. Eng.* **47** (2011) 125.
- 5 R. Liusheng, H. Liang, and P. Yongjun: *Int. J. Mach. Tool Des. Res.* **26** (2010) 87.
- 6 J. H. Shaik and J. Srinivas: *Sādhanā* **45** (2020) 55. <https://doi.org/10.1007/s12046-020-1286-7>
- 7 C. P. Reddy and S. S. Rao: *J. Eng. Ind.* **100** (1978) 137. <https://doi.org/10.1115/1.3439401>
- 8 S. S. Rao and R. V. Grandhi: *J. Mech. Trans. Autom.* **105** (1983) 236. <https://doi.org/10.1115/1.3258515>
- 9 S. J. Lee and S. G. Kapoor: *J. Eng. Optim.* **10** (1986) 25. <https://doi.org/10.1080/03052158608902525>
- 10 T. Prakosa, A. Wibowo, and R. Ilhamsyah: *J. Kones.* **20** (2013) 363.
- 11 G. Lei, Z. Hui, and Y. Peiqing: *J. Tsinghua Univ.* **51** (2011) 846.
- 12 K. Jie: *J. Hum. Univ. Arts Sci.* **26** (2014) 46.
- 13 Y. Guodong, Y. Wang, and X. Zhao: *Adv. Mech. Eng.* **10** (2018) 1. <https://doi.org/10.1177/1687814018813054>
- 14 Y. Wang, G. D. Wang, S. Zhang, Z. Tang, L. Wang, and Y. Liu: *Chin. J. Aeron.* **35** (2022) 485. <https://doi.org/10.1016/j.cja.2021.04.001>
- 15 J. Liu, Y. Cai, H. Zhang, and L. Ding: *E3S Web Conf.* **252** (2021). <https://doi.org/10.1051/e3sconf/202125202036>
- 16 Z. Lin, W. Tian, D. Zhang, W. Gao, and L. Wang: *Int. J. Adv. Manuf. Technol.* (2021). <https://doi.org/10.21203/rs.3.rs-893966/v1>
- 17 T. N. Ta, Y. L. Hwang, and J. H. Horng: *Int. J. Comp. Meth.* (2021) 2150028. <https://doi.org/10.1142/S0219876221500286>
- 18 H. Wu, X. Li, and F. Sun: *Int. J. Adv. Manuf. Technol.* **118** (2022) 1793. <https://doi.org/10.1007/s00170-021-07992-6>
- 19 K. C. Wang, C. H. Yang, L. Wu, and H. Gao: *Sens. Mater.* **32** (2020) 1633. <https://doi.org/10.18494/SAM.2020.2681>
- 20 S. Srinivasan and B. Subramanyam: *Imper. J. Interdiscipl. Res. (IJIR)* **2** (2016) 2454.
- 21 W. H. Yang and Y. S. Tarn: *J. Mater. Proc. Technol.* **84** (1998) 122. [https://doi.org/10.1016/S0924-0136\(98\)00079-X](https://doi.org/10.1016/S0924-0136(98)00079-X)
- 22 S. Moaveni: *Finite Element Analysis (Global Edition, 2014)* (Prentice Hall, Inc., New Jersey, 2014) 4th ed.
- 23 R. Mahdavinjad: *Int. J. Mach. Tools Manuf.* **45** (2005) 753. <https://doi.org/10.1016/j.ijmachtools.2004.11.017>
- 24 J. J. Wu: *Int. J. Mech. Sci.* **46** (2004) 1245. <https://doi.org/10.1016/j.ijmecsci.2004.07.002>
- 25 J. Heng, G. Yisheng, and Q. Zhicheng: *J. Mech. Eng.* **47** (2011) 125.
- 26 S. Yang: *Int. J. Mach. Tool Des. Res.* **21** (1981) 23. [https://doi.org/10.1016/0020-7357\(81\)90011-1](https://doi.org/10.1016/0020-7357(81)90011-1)
- 27 J. Majerik and J. Jambo: *Procedia Eng.* **100** (2015) 450. <https://doi.org/10.1016/j.proeng.2015.01.390>
- 28 E. Wagner: *Procedia Eng.* **19** (2015) 34. <https://doi.org/10.1016/j.proeng.2015.02.006>
- 29 D. Kano, T. Lorenzer, S. Weikert, and K. Wegener: *Precis. Eng.* **34** (2010) 399. <https://doi.org/10.1016/j.precisioneng.2009.09.003>
- 30 J. J. Wu: *Measurement* **39** (2006) 740. <https://doi.org/10.1016/j.measurement.2006.03.002>
- 31 Y. Kang, Y. P. Chang, J. W. Tsai, S. C. Cheng, and L. K. Yang: *Fin. Elem. Anal. Des.* **37** (2001) 485. [https://doi.org/10.1016/S0168-874X\(00\)00049-4](https://doi.org/10.1016/S0168-874X(00)00049-4)
- 32 K. Vivekananda, G. N. Arka, and S. K. Sahoo: *Procedia Mater. Sci.* **6** (2014) 1906. <https://doi.org/10.1016/j.mspro.2014.07.22314>
- 33 C. C. Hong, C. L. Chang, and C. Y. Lin: *Eng. Sci. Tech.* **19** (2016) 1971. <https://doi.org/10.1016/j.jestch.2016.07.013>
- 34 J. L. Deng: *The J. Grey Syst.* **1** (1984) 1.